Microstructure, Strength, and Wear Behavior Relationship in Al-Fe$_3$O$_4$ Nanocomposite Produced by Multi-pass Friction Stir Processing

Meisam Eftekhari, Mojtaba Movahedi, and Amir Hossein Kokabi

Aluminum matrix in situ nanocomposite was produced by one to six passes friction stir processing (FSP) with pre-placed Fe$_3$O$_4$ nanoparticles (15-20 nm). Microstructure studies showed that solid-state reactions between the aluminum matrix and Fe$_3$O$_4$ particles during the process led to in situ formation of Al$_3$Fe and Al$_5$Fe$_2$ in the stir zone. Initial Fe$_3$O$_4$ as well as Al-Fe intermetallic compounds (IMCs) particles were homogeneously dispersed in a fine grain matrix after six passes of FSP. Hardness and ultimate tensile strength of the composites were increased 64 and 27%, respectively, compared to the base metal. The reasons were studied in the light of reinforcing particles distribution, formation of Al-Fe IMCs, and grain size of the aluminum matrix. Pin-on-disk wear test indicated that in comparison with the base metal, the weight loss and friction coefficient of the composite processed by six passes decreased about 70 and 37%, respectively. Impact energy of the composite produced by six passes was considerably higher than that of the composite produced by one pass and reached to ~65% of the impact energy of the annealed aluminum base metal. Moreover, corrosion potential in the composites changed to more noble potentials compared to the base metal.

1. Introduction

Aluminum matrix composites (AMCs), reinforced with high hardness particles, are remarkable due to their good strength-to-weight ratio, high elastic modulus, and hardness. These properties, along with high wear resistance, have caused that AMCs are used in various fields such as automotive, aerospace, and defense industries (Ref 1-3). There are several techniques for fabrication of surface AMCs; the most important ones can be considered as plasma spraying (Ref 4) and cladding by high-energy beams (Ref 5). In the mentioned methods, due to presence of liquid phase, detrimental reactions between reinforcement and metal matrix and formation of cast defects may lead to undesirable mechanical properties (Ref 6). Therefore, researchers have focused on development and optimization of solid-state processes.

Friction stir processing (FSP) is a solid-state process developed by Mishra et al. (Ref 7) based on the principles of friction stir welding (FSW). In FSP a non-consumable rotating tool with a specially designed pin and shoulder is inserted into the workpiece for microstructure modification and traversed along the desired line. Heat generation by (a) friction between the rotating tool and the workpiece and (b) plastic deformation of the workpiece, softens the material around the pin and makes the material flow easier (Ref 7-10).

In general, two kinds of powders are used for fabrication of AMCs: ceramic reinforcements and metallic powders. Ceramic reinforcements usually are used for increasing the hardness of the materials directly (Ref 11-13). For instance, Mishra et al. (Ref 11) used SiC for this purpose. In another research by Palanivel et al. (Ref 13), nanosized TiB$_2$ and BN, separately and together, were used to improve wear behavior of aluminum. On the other hand, metallic powders are usually used to react with aluminum matrix during the process and form intermetallic compounds (IMCs) which they increase the hardness of the composites (named as in situ composites). The advantages of in situ composites may be more homogeneous microstructures and stronger interfacial bonding between reinforcing particles and the aluminum matrix (Ref 14, 15). Since FSP is a thermo-mechanical process in which material experiences severe plastic deformation as well as high temperature, reaction between the matrix and reinforcing particles is expected to be promoted. However, formation of thick brittle intermetallic phases between the metallic reinforcements and the aluminum matrix especially during the service of the composite at high temperatures can be detrimental to mechanical properties. On the other hand, since ceramic reinforcements have higher hardness compared with metallic ones, they may lead to superior strengthening effect in the composite.

Al-Fe composites have been previously fabricated by different methods such as plasma synthesis (Ref 16), mechanical alloying (Ref 17), and FSP with and without preceding powder metallurgy approach (Ref 18, 19). Lee et al. (Ref 18) used FSP to produce aluminum-based nanocomposite after preceding powder metallurgy technique from powder mixture of Al-10 at.% Fe. The examination of the microstructure revealed that the reaction between aluminum and iron during powder metallurgy and FSP led to formation of Al-Fe

Meisam Eftekhari, Mojtaba Movahedi, and Amir Hossein Kokabi, Department of Materials Science and Engineering, Sharif University of Technology, P.O. Box 11365-9466, Azadi Avenue, Tehran 14588, Iran. Contact e-mail: m_movahedi@sharif.edu.

intermetallic compounds, i.e., Al_3Fe ($Al_{13}Fe_4$) and Al_5Fe_2. In another research done by Sarkarikhorrami et al. (Ref 19), Al-1050 sheets were processed by FSP using pre-placed Fe particles in a groove along the sample to produce aluminum matrix composite. They observed IMCs in their samples which formed from reaction of aluminum and iron. They also reported that improvement in the distribution of Fe particles and enhancement of IMCs led to increase in the ultimate tensile strength (UTS) of the composites.

In this work, Al matrix/Fe_3O_4 nanopowder composite was produced using FSP. Fe_3O_4 nanopowders can increase the hardness and strength of the Al matrix directly. They may also react with aluminum matrix and form Al-Fe IMCs increasing the hardness of the stir zone. Thus, the objective of the work was investigation of the ability of FSP method for fabrication of aluminum matrix in situ composite using Fe_3O_4 nanopowders. Moreover, effects of FSP pass number on microstructure and mechanical properties of the composite were explored.

2. Experimental Procedures

Al-1050 commercially pure aluminum sheets with the weight composition of Al-0.24 Fe-0.07 Si-0.02 Mn-0.01 Mg-0.01 Zn-0.01 Ti-0.01 V and dimensions of $150 \times 70 \times 4$ mm and Fe_3O_4 nanoparticles with the size at the range of 15-20 nm and 99.5% purity, were used as the starting materials. Chemical composition of the aluminum sheet was determined by optical emission spectroscopy. The very small size of particles in
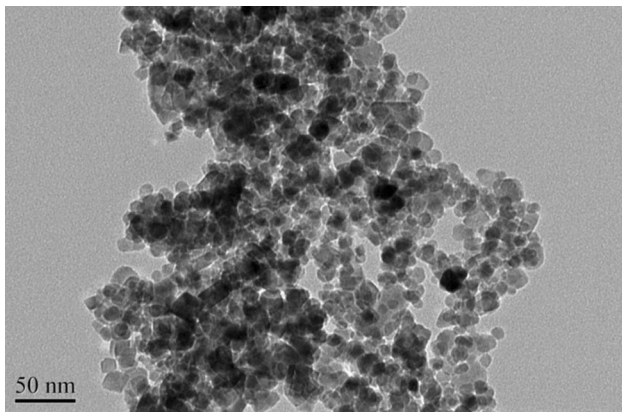
**Fig. 1** TEM image of Fe_3O_4 nanoparticles presented by the provider company (Ref 20)

nanosized Fe_3O_4 may facilitate the reduction of iron oxide to Fe as well as the subsequent formation of Al-Fe intermetallics through solid-state reactions during the process. Figure 1 presents the transmission electron microscope (TEM) image of the Fe_3O_4 nanoparticles presented by the provider company (Ref 20). The as-received aluminum sheets were fully annealed at 425 °C for 75 min. The mechanical properties of the annealed aluminum are given in Table 1.

A groove was machined at the center of the aluminum base sheets with a length, width, and depth of 150, 1, and 3 mm, respectively. After inserting about 0.6 g of Fe_3O_4 nanoparticles inside the groove, a rotating free-pin tool was used to close the surface of the groove for preventing the Fe_3O_4 nanoparticles from throwing out of the groove during FSP. The FSP tool was made from a heat-treated H-13 tool steel with a hardness of 52-54 RC. Shoulder and pin diameters, pin length, and tilt angle of the tool were 20, 5, 3.4 mm and 3°, respectively. The traverse and rotation speeds of the tool and plunge depth of the shoulder were also adjusted at 10 cm/min, 1400 rpm, and ~0.2 mm, respectively. Samples were produced with 1, 2, 3, and 6 passes of FSP. It is worth mentioning that the direction of the tool rotation was changed in each pass in order to obtain a homogeneous distribution of the powders as well as the grain structure through the stir zone. Since the advancing side of the stir zone experiences higher temperature and more stirring action compared with retreating side, there is heterogeneity between the microstructure of these regions (Ref 7, 19). Changing the direction of the tool rotation, or in fact changing the advancing and retreating sides in each pass, may lead to more uniform microstructure through the stir zone. Moreover, given the weight of the particles used in each sample as well as the geometry of the stir zone obtained from cross-sectional images, the weight percent of the produced composites was calculated about 2.5%. For this purpose, the cross section of the stir zone was obtained using ImageJ software. Then the volume (cross section × length of the sample) and mass (cross section × length of sample × aluminum density) of the stir zone were determined. The weight percent of the composites was approximately calculated as mass of the inserted Fe_3O_4 nanoparticles (0.6 g) divided by the mass of the stir zone (23-25 g).

In order to investigate the mechanical properties of the obtained composites, transverse and longitudinal tensile tests and Vickers microhardness test along with the wear test were performed. Tensile test specimens were prepared according to the subsize sample of the ASTM E8-M standard with the dimensions shown in Fig. 2(a). Transverse tensile test was carried out to compare the UTS of the various processed zone (i.e., stir zone, thermo-mechanically affected zone, and heat

Table 1 Grain size and mechanical properties of the Al-1050 base metal and produced composites

	Grain size, μm	Hardness, Vickers	YS, MPa	UTS, MPa	Elongation, %		
Al-1050 base metal	70 ± 6	22 ± 2	33 ± 2	66 ± 4	44 ± 5		

			Longitudinal tensile test			Transverse tensile test		
Composite	Grain size, μm	Hardness, Vickers	YS, MPa	UTS, MPa	Elongation, %	YS, MPa	UTS, MPa	Elongation, %
1 pass	12.1 ± 0.6	26 ± 5	34 ± 3	49 ± 3	5 ± 2	35 ± 3	47 ± 4	5 ± 3
2 passes	9.8 ± 0.8	29 ± 7	37 ± 4	62 ± 5	13 ± 1	35 ± 2	58 ± 3	9 ± 2
3 passes	5.9 ± 1.2	32 ± 6	41 ± 2	72 ± 3	12 ± 3	33 ± 3	68 ± 2	13 ± 4
6 passes	4.2 ± 0.5	36 ± 5	46 ± 2	84 ± 4	10 ± 2	31 ± 4	67 ± 2	15 ± 4
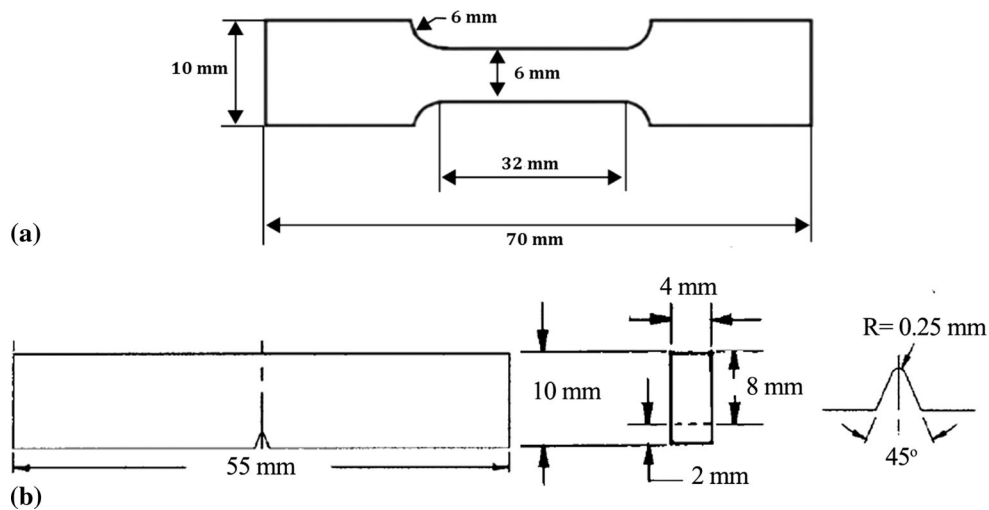
Fig. 2 Dimensions of (a) tensile test and (b) impact test samples

affected zone) with the base metal. Thus, transverse tensile specimens were extracted from the FSPed samples so that the stir zone was placed at the center of the gage length. Longitudinal tensile test was performed for evaluation of the mechanical behavior of the stir zone, and given this purpose, longitudinal tensile specimens were cut from the center of the stir zone. Tensile tests were performed by an Instron machine with the crosshead speed of 1 mm/min. The Vickers microhardness was measured using 200 g load for 15 s. The microhardness measurements were taken along a line which was 2 mm under the surface of the specimens from the stir zone toward the base material.

Tribological behavior of the composites was examined using pin-on-disk wear test based on ASTM G99-04 standard. Cylindrical pins with the diameter of 3 mm were extracted from the stir zone of the samples as well as the base metal parallel to the longitudinal direction of the samples. SPK steel (C = 1.2080 wt.%, Cr = 12 wt.%, Fe = bulk) was used as the counterpart disk with the diameter of 50 mm, thickness of 7 mm, and hardness of 700 Hv. Wear test was performed in a dry sliding condition under a constant load of 30 N, sliding velocity of 0.28 m/s, and sliding distance of 500 m. All worn-out pins were cleaned in acetone and weighed to an accuracy of ±1 mg and the weight loss was measured. The coefficient of friction between pin and disk was determined by measuring the frictional force.

Charpy V-notch tests were performed to evaluate impact toughness of the aluminum base metals and produced composites at the temperature of 25 °C. The subsize samples with the dimensions of 4 mm in thickness, 10 mm in width, and 55 mm in length were used in accordance with ASTM E23 standard. The schematic and dimensions of the impact test samples are shown in Fig. 2(b).

To investigate the effect of Fe_3O_4 reinforcements on the corrosion behavior of the produced composites, Tafel plots of the aluminum base metal as well as the composites processed by 1 and 6 passes were recorded in 3.5 wt.% NaCl solution with the scan rate of 1 mV s^{-1}. Polarization measurements were carried out using a potentiostat/galvanostat AUTOLAB model PGSTAT302N equipped with Nova1.5 software. All experiments were done in a typical three-electrode cell with saturated calomel electrode (SCE) and SS316 sheet as reference and counter electrodes, respectively.

Microstructure of the stir zone was examined by optical microscopy (OM) using polarized light. For this purpose, the cross sections of FSPed specimens were prepared by standard metallographic procedures and then electro-etched by the solution of 100 mL HBF$_4$ (2.5%) + 10 mL HF at voltage of 10 V for 60 s and then 20 V for 90 s. The average grain sizes of the base metal and stir zones of the composites were measured using general intercept procedure according to ASTM E 112 standard. Three different regions were evaluated for each sample and the mean values and standard deviations were reported. Moreover, distribution of Fe_3O_4 nanoparticles inside the stir zone was studied using field emission scanning electron microscopy (FESEM). FESEM was also used to study the fracture surfaces of the composites obtained from longitudinal tensile tests. In order to detect Al-Fe IMCs at the interface of Fe_3O_4 nanoparticles and aluminum matrix, FESEM equipped with energy-dispersive spectroscopy (EDS) was employed.

3. Results and Discussion

3.1 Microstructure

3.1.1 Fe_3O_4 Distribution and Formation of Intermetallics. FESEM images from the stir zone of the specimens processed by 1, 3, and 6 passes of FSP with Fe_3O_4 particles are shown in Fig. 3. As can be seen, agglomeration of particles decreased with increase in FSP pass number. In other words, the more was the FSP pass number, the more uniform was the distribution of Fe_3O_4 particles. In the first pass, iron oxide powders which have lower formability than aluminum matrix were concentrated inside the groove, so their flow was difficult and most of them remained at the center of the stir zone (Fig. 3a). However, with enhancement of the pass number, they could move around in the stir zone resulting in less agglomeration and more uniform distribution of the particles (Fig. 3c). On the other hand, poor bonding and cracks between the severely agglomerated particles and the surrounding aluminum matrix were observed in the specimen processed by 1 pass (Fig. 3a). In fact, due to lack of material flow around the agglomerated particles, cracks and discontinuities were formed
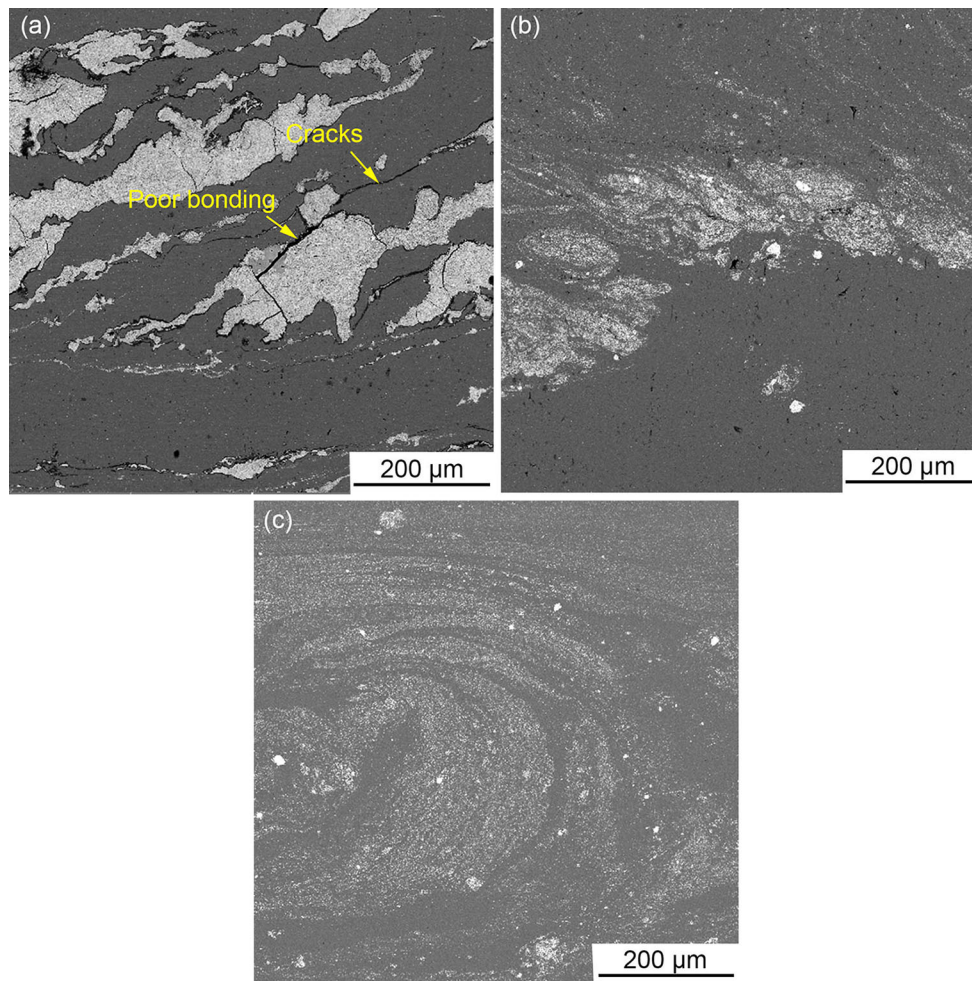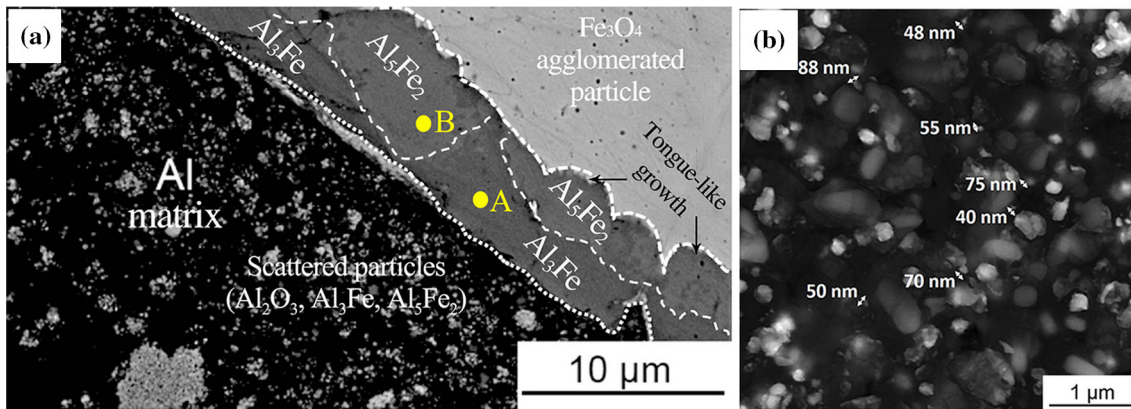
Fig. 3 FESEM image from the center of the stir zone showing distribution of Fe_3O_4 nanoparticles in the specimens processed by: (a) 1 pass, (b) 3 passes and (c) 6 passes

around the particles inside the stir zone. However, these defects were removed with increase in the pass number (Fig. 3b and c) since the size and number of agglomerated particles decreased.

Another issue investigated in this research was the possibility of the formation of in situ Al-Fe intermetallics from the reaction between aluminum and iron oxide nanopowders during FSP. There are five Al-Fe intermetallic compounds, i.e., $AlFe_3$, $AlFe$, Al_2Fe, Al_5Fe_2, and Al_3Fe ($Al_{13}Fe_4$), in Al-Fe phase diagram. According to Ellingham–Richardson diagram (Ref 21), aluminum has more tendencies to react with oxygen in comparison with iron at the temperature range of aluminum FSP. Consequently, it was expected that iron oxide would be reduced by aluminum and then by the stirring action of the rotating tool; metallic iron would be situated at the contact with the aluminum matrix. On the other hand, there is thermodynamically tendency between aluminum and iron to react with each other and form Al-Fe IMCs due to the negative free energy of formation for various Al-Fe intermetallics (Ref 16). Therefore, FESEM was used to investigate the interface of the iron oxide particles and the aluminum matrix. Figure 4(a) shows the interface of an agglomerated iron oxide particle and the adjacent aluminum in the stir zone of the composite processed by 6 passes. It is clear that a reaction layer with thickness of $\sim$5 μm was formed around an agglomerated Fe_3O_4 particle. Given the high thickness of the intermetallic layer at

the interface, it can be concluded that the nanometer particles react completely with the aluminum matrix and transform to the Al-Fe IMCs. Looking carefully at Fig. 4(a), the reaction layer consisted of two parts. On the other hand, the EDS analysis result presented in Table 2 verified the formation of Al_3Fe and Al_5Fe_2 adjacent to the Al matrix and Fe_3O_4 particle, respectively. Based on the previous researches, Al_5Fe_2 (with tongue like growth) and Al_3Fe ($Al_{13}Fe_4$) are the most common IMCs which form in the diffusion couples between Al and Fe (Ref 18, 22, 23). Movahedi et al. (Ref 22) investigated the growth kinetics of Al-Fe IMCs during post-weld annealing of the aluminum-steel lap joints and reported that there were two different IMCs at the weld interface. They used electron backscattered diffraction (EBSD) analysis and concluded that the layer adjacent to the steel was Al_5Fe_2 and the other one was Al_3Fe. In another research carried out by Xingqing et al. (Ref 23), two phases of Al_5Fe_2 and Al_3Fe were identified at the interface of iron and aluminum. These IMCs with high hardness ($Al_3Fe = \sim$717 Hv, $Al_5Fe_2 = \sim$944 Hv) (Ref 16) are broken during the FSP due to the stirring action of the tool and distributed inside the aluminum matrix. Figure 4(b) shows the stir zone in the specimen processed by 6 passes. As can be seen, three distinct phases with different contrast can be distinguished. The brightest phases were Fe_3O_4 particles, while the dark matrix was Al. The gray phases surrounding the Fe_3O_4

Fig. 4 FESEM image from (a) interface of Al matrix and Fe_3O_4 agglomerated particles and (b) the broken and scattered nanometric particles in the stir zone of the composite processed by 6 passes

Table 2   EDS analysis results of the IMCs formed at the matrix/particle interface

| Location in Fig. 3(a) | Al (wt.%) | | Identified IMC |
	Measured composition	Nominal composition	
A	63	Al_3Fe: 58.5-61	Al_3Fe
B	54	Al_5Fe_2: 53.5-56	Al_5Fe_2

particles or dispersed in the Al matrix were Al-Fe IMCs. Nanometer particles (broken intermetallics and/or Fe_3O_4 powders) are shown in Fig. 4(b).

3.1.2 Grain Structure. Figure 5(a) shows the grain structure of the annealed base metal consisting of equiaxed grains with an average grain size of ~70 μm. Figure 5(b), (c), (d), and (e) also shows the grain structure of the composites processed by 1 to 6 passes. Moreover, the average grain size of the stir zone in composites is given in Table 1. As can be seen, with increase in the pass number, the grain size of the stir zone decreased. After one pass of FSP, dynamic recovery/recrystallization occurred in the stir zone (Ref 7) and resulted in finer grain structure in comparison with the annealed base metal. However, during the process, heat is generated due to the friction between the tool and the workpiece as well as the severe plastic deformation leading to the grain growth after dynamic recrystallization. On the other hand, submicron particles as shown in Fig. 4 may act as barriers to the movement of grain boundaries and therefore hinder the growth of the grains. So presence of nanometer particles may result in finer grain structure. This phenomenon is known as Zener pinning mechanism. The research done by Hansen and Bay (Ref 24) on the recrystallization and grain size of aluminum containing both coarse (0.2-4 μm) and fine (<0.1 μm) secondary particles showed that coarse particles are suitable places for nucleation [known as particle stimulated nucleation (PSN) mechanism] due to presence of stress concentration and high dislocation density around them (Ref 25). However, fine particles are not considered as very high-energy places, so they do not encourage nucleation. It was observed that aluminum with nano- and submicron particles had finer grains in comparison with the aluminum with coarse particles. This was related to the prevention of grain growth by fine particles. So presence of nanometer particles may result in finer grain structure (Ref 25-27). In the first pass of FSP in this study, Zener pinning mechanism was not very effective due to

agglomeration of the reinforcing particles. But with increase in the pass number to 6 passes, aggregation of the particles decreased and their distribution got more uniform. The well-distributed nano- and submicron particles hampered extended grain growth, and therefore, the microstructure of the stir zone composed of finer grains in comparison with the stir zone of the samples processed by lower pass number. Non-uniform distribution of the reinforcing particles can cause abrupt grain structure changes in the stir zone. It is shown in Fig. 5(f) and (g) that the areas with higher weight percent of Fe_3O_4 had a finer grain structure (an average grain size of ~2 μm) compared to areas with lower one (an average grain size of ~10 μm). The grain size reported in this study in Table 1 was the average size of both coarse and fine grain regions. However, with increase in the pass number to 6 passes, the composite had more uniform grain structure without abrupt changes in the grain size at the various regions in the stir zone.

3.2 Mechanical Properties

3.2.1 Microhardness. Figure 6(a) shows the results of microhardness measurements. As can be seen, the hardness of stir zone increased in the FSPed specimens in comparison with the base metal. In addition, enhancement of the pass number led to the increase in the average hardness in the stir zone. In the specimen with the highest hardness, i.e., specimen processed by 6 passes, the average hardness in the stir zone increased about 64% compared to the base metal. Finer grains, superior distribution of Fe_3O_4 particles, and formation of more Al-Fe intermetallic compounds due to increase in heat input in each pass are the main reasons.

3.2.2 Transverse and Longitudinal Tensile Tests. Figure 7 shows the stereographs from fractured specimens after transverse and longitudinal tensile test. While the specimens processed by 1 and 2 passes were fractured during transverse tensile test from the stir zone, failure in the specimens
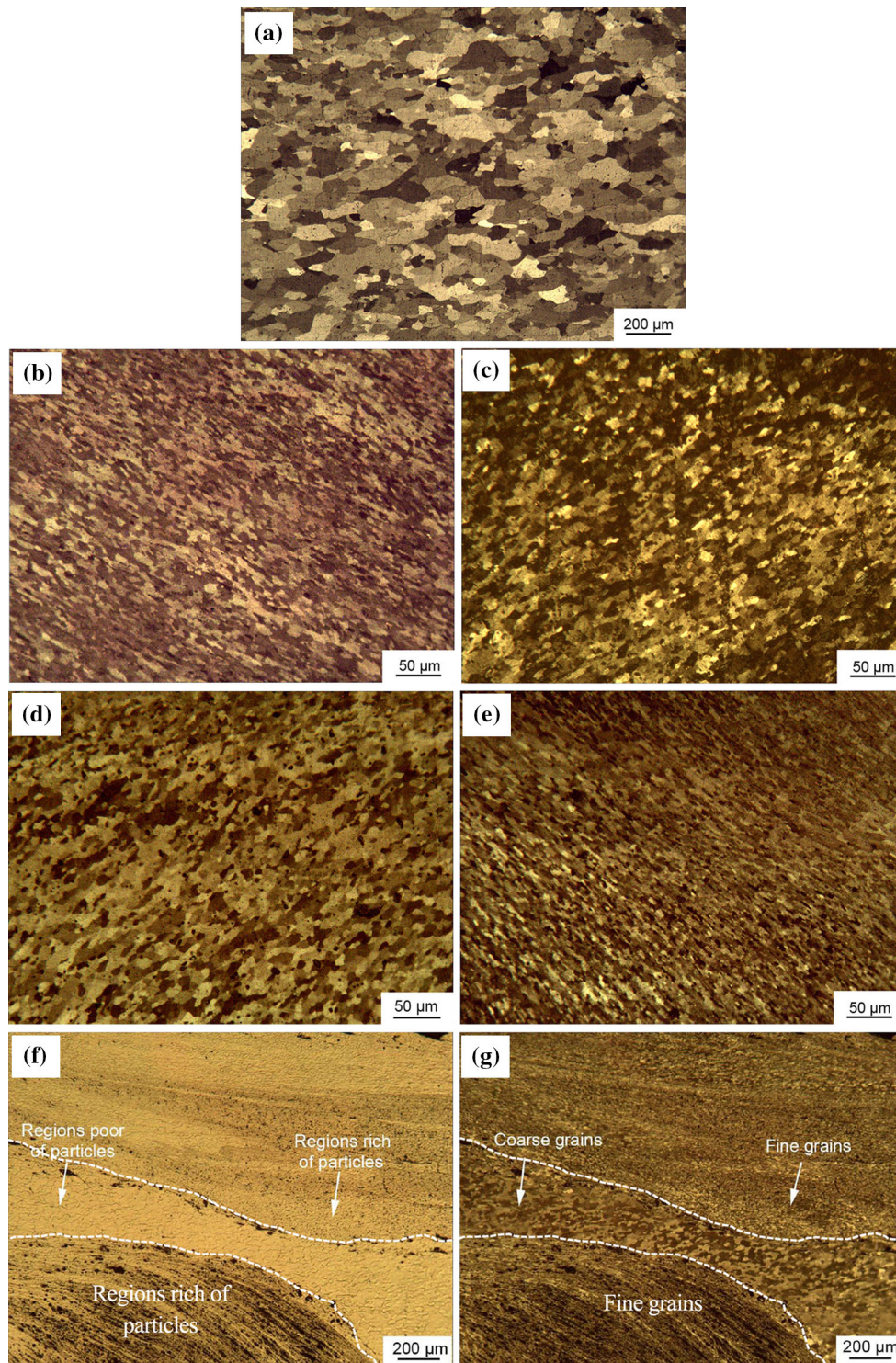
Fig. 5 Optical microscope images showing the microstructure of the (a) base metal, and stir zone of the specimens processed by: (b) 1 pass, (c) 2 passes, (d) 3 passes and (e) 6 passes. (f) and (g) show the fine and coarse grains regions in the stir zone of 3 passes specimen before and after etching, respectively

processed by 3 and 6 passes occurred from the base metal. The mentioned phenomena confirm that contrary to the specimens processed by 1 and 2 passes, UTS of the stir zone for the samples processed by 3 and 6 passes was higher than that of the base metal (Table 1). The reasons for the superior tensile strength of the stir zone in the samples processed by higher pass number will be discussed later.

Figure 6(b) shows the stress-strain curves for the longitudinal tensile test from the aluminum base metal as well as the composites undergone various passes of FSP. As can be seen, UTS increased with raising the pass number and the uniformity of the reinforcing particles in the structure. In the specimen processed by 6 passes, UTS increased by 27% compared to the
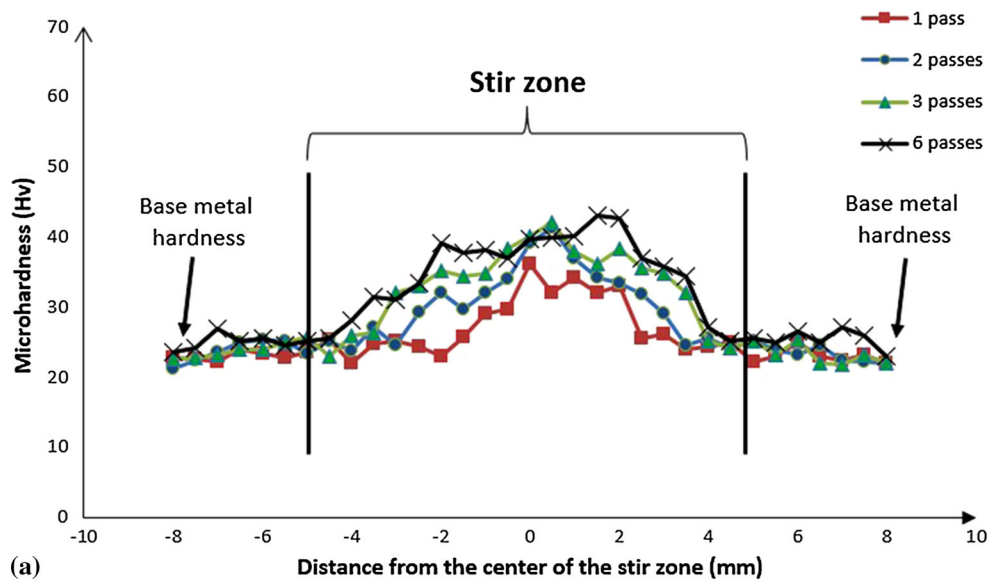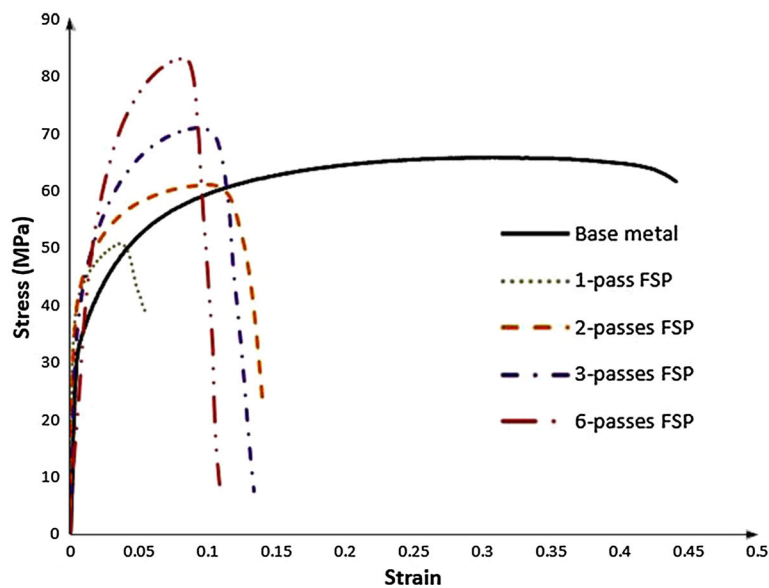
Fig. 6 Mechanical behavior of the composites, (a) hardness profile along the centerline of the sample cross section and (b) stress-strain curves obtained from longitudinal tensile tests

base metal. Generally, three factors are effective on the lower tensile strength of the composites processed by 1 and 2 passes:

1. agglomeration of the reinforcing particles,
2. presence of voids and cracks in the stir zone caused by poor bonding between the agglomerated particles and aluminum matrix as discussed in section 3.1.1
3. lower amount of Al-Fe IMCs due to the lesser heat input and more agglomeration of the Fe_3O_4 powders.

Agglomeration of the particles and presence of voids and cracks in the specimens processed by 1 and 2 passes caused stress concentration and so, fracture occurred with forces lower than that required for the fracture from the base metal. However, by enhancement of the pass number to 3 and 6 passes and elimination or reduction in the particles agglomeration, voids, and cracks, the strength of the stir zone increased to values higher than the strength of the aluminum base metal.

Sarkarikhorrami et al. (Ref 19) produced Al-1050/4 wt.% Fe composite by FSP. They used Fe powders with ∼10 μm average size. The UTS of the composite fabricated via three passes of FSP reached to 90 MPa that is comparable to the UTS of the composite produced by six passes (∼85 MPa) in the present work. However, the composites in this research composed of ∼2.5 wt.% reinforcing particles. In another work, the UTS and elongation of an aluminum-based nanocomposite produced using four passes of FSP after preceding powder metallurgy technique from powder mixture of Al-18 wt.% Fe reached up to 217 MPa and 3.6%, respectively (Ref 18). The superior strength and lower elongation of this composite compared to the composites fabricated in the present study may be attributed to the significant higher weight percent of the reinforcing particles. Lee et al. (Ref 18) also reported uniform distribution of the ∼100 nm Al-Fe intermetallics inside the aluminum matrix that can be effective in higher strength of the nanocomposites produced in their work. Gu et al. (Ref 17)
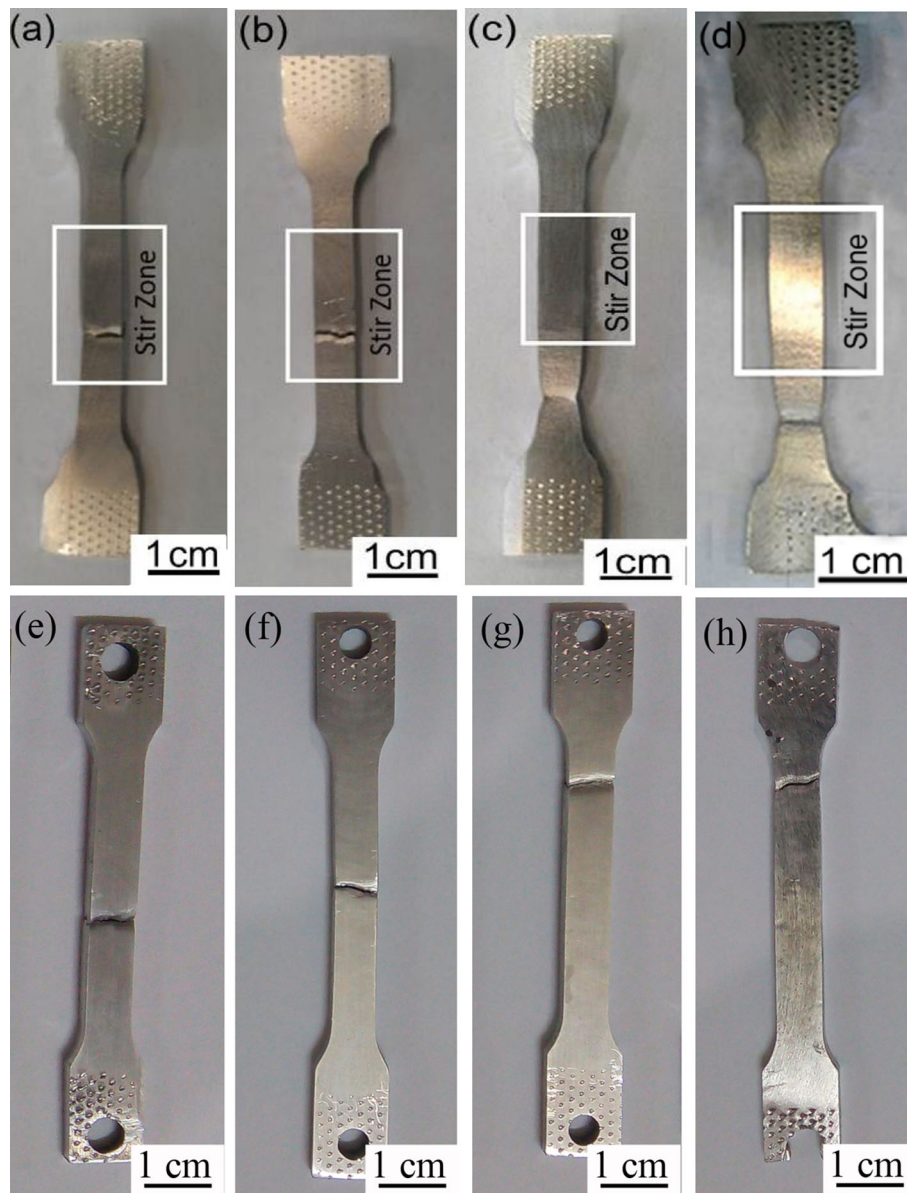
Fig. 7 (a–d): stereographs after transverse tensile test of the specimens processed by (a) 1 pass, (b) 2 passes, (c) 3 passes, and (d) 6 passes of FSP, (e–h): stereographs after longitudinal tensile test of the specimens processed by (e) 1 pass, (f) 2 passes, (g) 3 passes, and (h) 6 passes of FSP

studied the mechanical properties of the composites of Al-Fe alloys containing 4-18 wt.% Fe fabricated by mechanical alloying for 80 h and subsequent spark plasma sintering as a fusion process. They obtained the yield strengths of ~500 to ~1100 MPa at the samples containing 4 to 18 wt.% Fe, respectively. High volume fraction of Al-Fe intermetallic (~10 to 35%) may be responsible for these high yield strengths compared to yield strengths obtained in the present research.

It is also observed that the elongations in all the composites (in longitudinal tests) were reduced in comparison with the base metal. Given the presence of Fe_3O_4 and intermetallic compounds which have a higher hardness compared to the aluminum base metal, increase in UTS and decrease in elongation is expectable. Fractography studies from longitudinal tensile test samples showed equiaxed and deep dimples (i.e., features of ductile fracture) for the specimen processed without Fe_3O_4 particles as shown in Fig. 8(a). The fracture

surfaces of the composites processed by 1, 3 and 6 passes of FSP are presented in Fig. 8(b), (c), and (d). In the specimen processed by 1 pass, there were obvious separations between agglomerated Fe_3O_4 particles and aluminum which implying the presence of defects at the particle-matrix interface and poor metallurgical bond between them. In addition, few dimples at the fracture surface show that brittle fracture was dominant in this specimen. The very low elongation of the sample processed by 1 pass (shown in Fig. 6(b) and Table 1) was in agreement with the dominance of brittle features on the fracture surface. In the specimens processed by 3 and 6 passes, a mixture of ductile and brittle features was observed on the fracture surfaces. This justifies the higher elongation of these specimens in comparison with the specimen processed by 1 pass. Results of the transverse tensile tests (Table 1) show that in the samples produced by 1 and 2 FSP passes in which fracture occurred inside the stir zone, elongation was lower than the samples
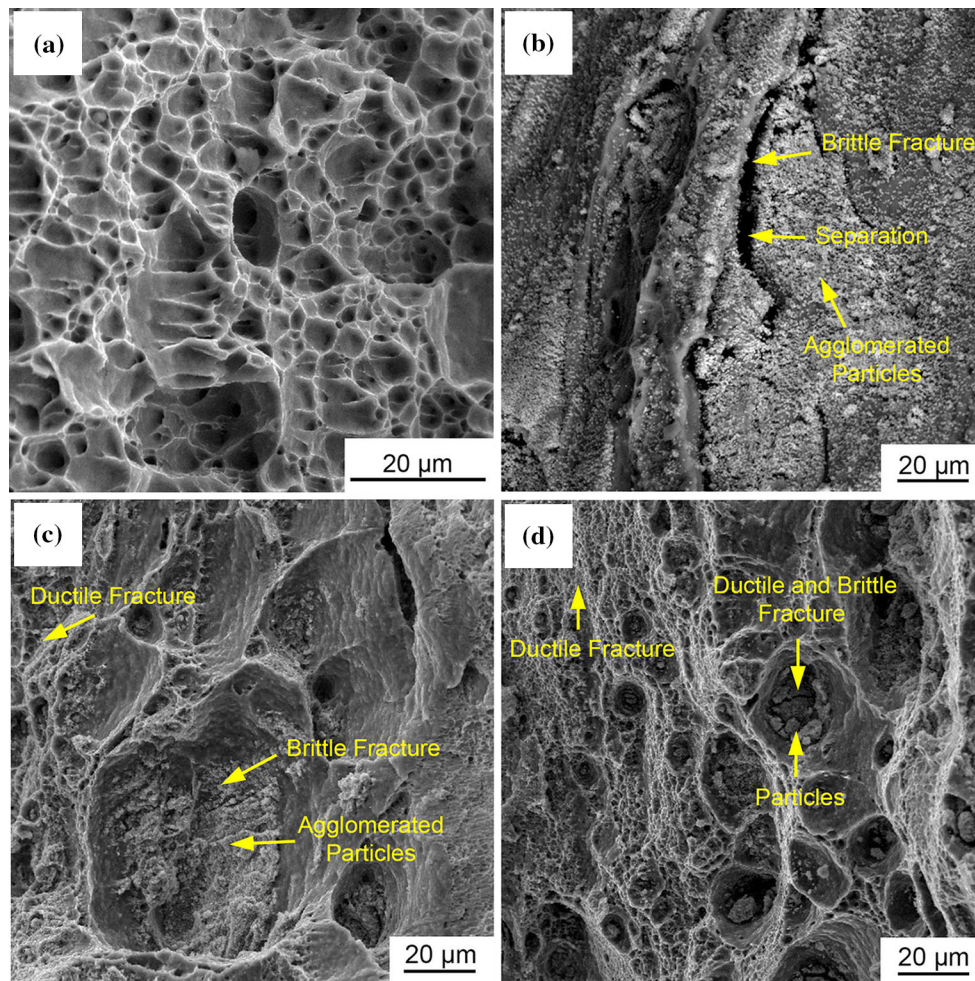
Fig. 8 FESEM image from the fracture surface of the specimen processed (a) without Fe_3O_4 particles, (b) by 1 pass, (c) by 3 passes, and (d) by 6 passes
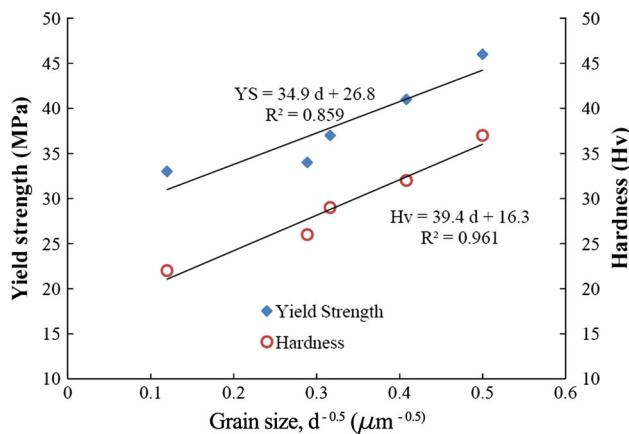
Fig. 9 Relationship between yield strength and Vickers hardness with average grain size

produced by 3 and 6 passes in which fracture occurred from the aluminum base metal. This may also be attributed to the more brittle nature of the composites compared to the aluminum base metal as discussed for longitudinal tensile tests.

Generally, in metallic materials, the yield strength (YS) is related to average grain size (d) according to Hall–Petch equation (Ref 28, 29) as follows:
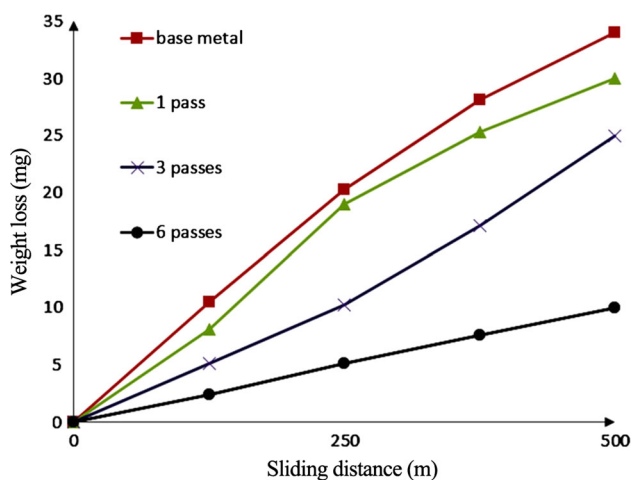
$$YS = Y_0 + k_1 d^{-0.5} \qquad \text{(Eq 1)}$$

where Y_0 and k_1 are friction stress (resistance of the crystal lattice to dislocation movement) and Hall–Petch coefficient, respectively. In the absence of work hardening in the material, hardness (H) may be related to yield strength as $H \approx 3$ YS (Ref 30). Hence, a linear relationship similar to Eq 1 is derived for the hardness of material as:

$$H = H_0 + k_2 d^{-0.5} \qquad \text{(Eq 2)}$$

where H_0 and k_2 are constants similar to Y_0 and k_1, respectively, but related to the hardness values. Yield strength and Vickers hardness via $d^{-0.5}$ for the aluminum base metal and the produced composites are depicted in Fig. 9. According to the linear trendlines fitted to the data, the values of Y_0, k_1, H_0, and k_2 were obtained as 26.8, 34.9 MPa $\mu m^{0.5}$, 16.3, and 39.4 Hv $\mu m^{0.5}$, respectively. The obtained Y_0 is at the range (15-30 MPa) reported by Shanmugasundaram et al. (Ref 31) for the commercially pure aluminum. However, the obtained Hall–Petch coefficient (k_1) is fewer than that reported in some previous researches on the commercially pure aluminum (60-

70 MPa $\mu m^{0.5}$) (Ref 31-33). This may be attributed to difference between grain size ranges in the samples investigated in this research (4-70 μm) by those studied in the references (nanosized and ultrafine grained structure) (Ref 31-33). Sato et al. (Ref 34) investigated the relationship between Vickers hardness and $d^{-0.5}$ in friction stir welds of equal channel angular pressed Al-1050 aluminum alloy. They reported that Hall–Petch coefficient for hardness (k_2) varies from ∼53 Hv $\mu m^{0.5}$ for average grain size fewer than ∼0.6 μm to ∼14 Hv $\mu m^{0.5}$ for average grain size beyond 0.6 μm. Coefficient of k_2 obtained in the present work (39.4 Hv $\mu m^{0.5}$) lies between the two values reported by Sato et al. (Ref 34) for ultrafine and coarse grained structures.

It is worth mentioning that the low values of R^2 (which shows how close the data are to the fitted linear trendline) especially for the yield strength data confirm that the yield strength and hardness values are not just determined by the grain size and therefore other phenomena control them. In the case of the composites produced in this study, presence of the reinforcing particles may affect the hardness and yield strength. Since the distribution and agglomerate size of the Fe_3O_4 particles as well as the formation of Al-Fe intermetallic compounds change by alteration of the pass number, the contribution of these particles in the hardness and yield strength of the composites varies. Therefore, the relationship between the hardness and yield strength with $d^{-0.5}$ deviates from a linear behavior.

Fig. 10 Weight loss of the base metal and the specimens FSPed by different passes
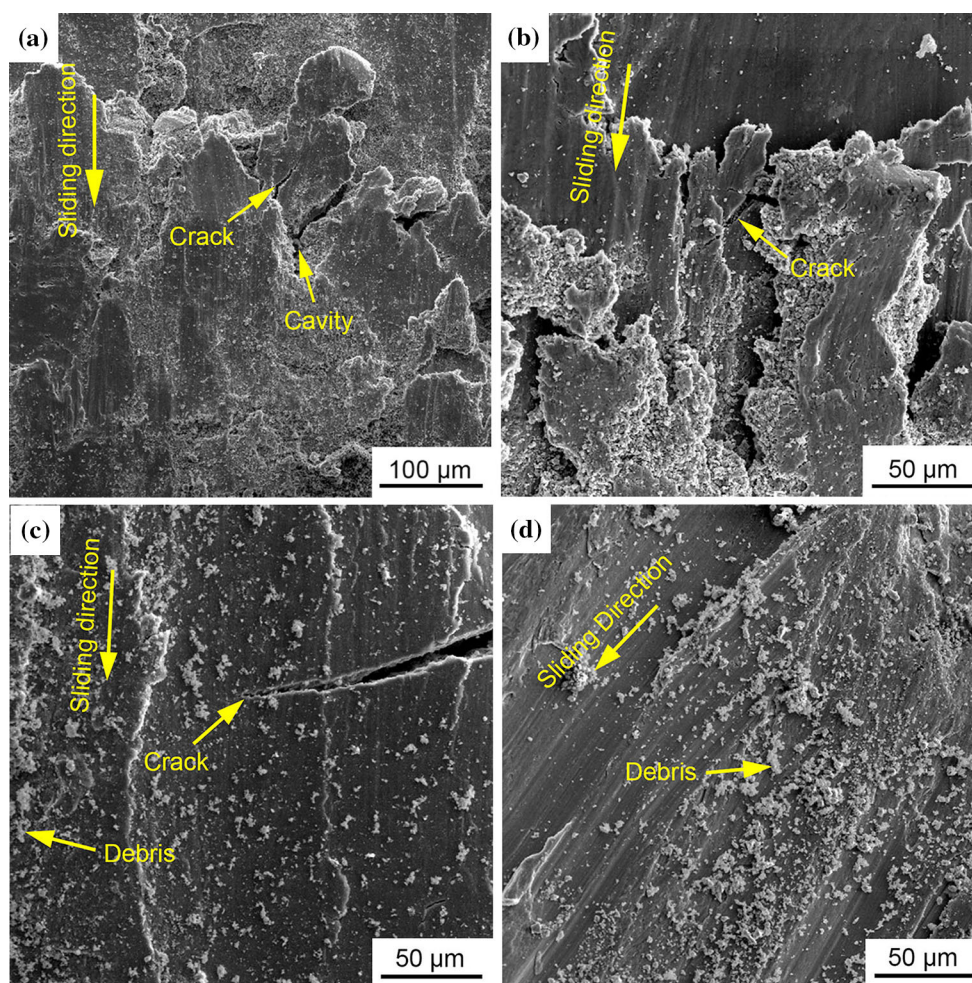
Fig. 11 FESEM image from the worn-out surface of (a) aluminum base metal, and specimens processed by (b) 1 pass, (c) 3 passes and (d) 6 passes
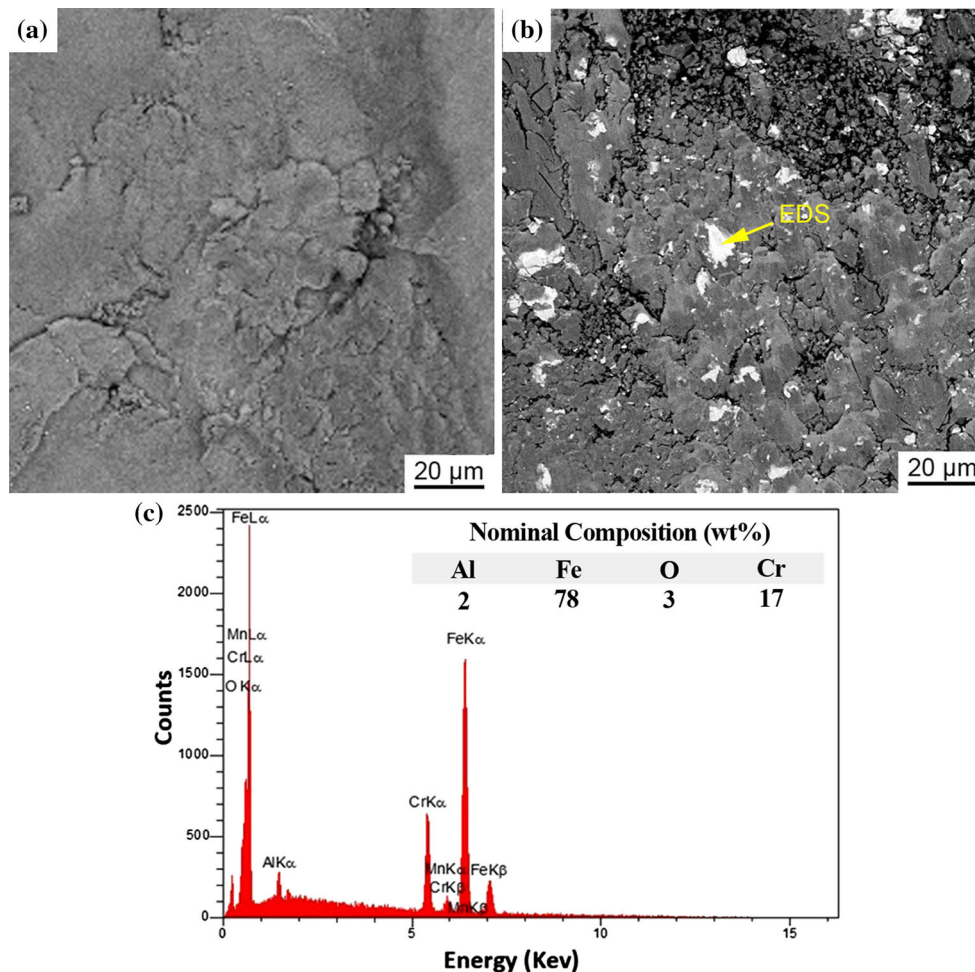
Fig. 12 FESEM image from the worn-out surface of the specimen processed by (a) 1 pass and (b) 6 passes of FSP. (c) EDS analysis and nominal composition of the debris shown by the arrow in (b)

3.2.3 Wear. The weight loss of the pin-shaped specimens as a function of sliding distance is presented in Fig. 10. As can be seen, the weight loss of FSPed specimens is lower than that of the base metal. However, the wear resistance in the specimen processed by 1 pass was close to the base metal because of the severe agglomeration and poor bonding between the agglomerated Fe_3O_4 particles and the aluminum matrix. Due to more uniform distribution of the particles and increase in the intermetallic compounds in the specimens processed by 3 and 6 passes, higher hardness and lower weight loss were obtained. In the specimen processed by 6 passes, the weight loss decreased about 70% compared to the base metal.

In order to understand the wear behavior of the composites during the wear test in more detail, the worn-out surface of the specimens were examined. The worn-out surface of the aluminum base metal is shown in Fig. 11(a). Presence of cracks and cavities is an evidence for severe plastic deformation on the surface and subsurface of the sample. In this severe wear mechanism, subsurface cracks initiate due to the imposed high shear stress during wear and presence of subsurface stress concentrations like inclusions or second phase particles. By continuing wear, cracks propagate parallel to the free surface of the sample. This process is well known as "delamination wear" (Ref 35-38). This mechanism is a dominant wear mechanism in soft materials and the composites which have a poor parti-

cle/matrix interfacial bonding (Ref 35, 36). Figure 11(b) shows the worn-out surface of the specimen processed by 1 pass. In this specimen, severe wear was also occurred with the evidence of the presence of cracks and delamination of the surface. Furthermore, separation and trapping of Fe_3O_4 particles between the pin and disk surfaces resulted in the "third-body wear." Separation of Fe_3O_4 particles from the aluminum matrix during the test was caused by poor bonding between agglomerated particles and the matrix as well as the formation of voids at the interface of the particle/matrix in the specimen processed by 1 pass as mentioned in section 3.1.1. However, in this specimen, it seems this wear mechanism was not very active due to high plastic deformation on the surface. In the other words, because of the low hardness of the specimen, delamination is still a dominant wear mechanism for this specimen. Furthermore, existence of debris in the samples processed by 3 and 6 passes indicated that third-body wear occurred in these specimens (Fig. 11c and d). With increasing the pass number, nanometric reinforcing particles were distributed more uniformly and as a result, crack propagation was hindered due to presence of submicron particles at the path movement of cracks. In addition, reinforcing particles may reduce surface deformation during wear test. In fact, these particles with higher strength than aluminum can withstand the applied load without much deformation. Thus, if the particles distribute finely, they
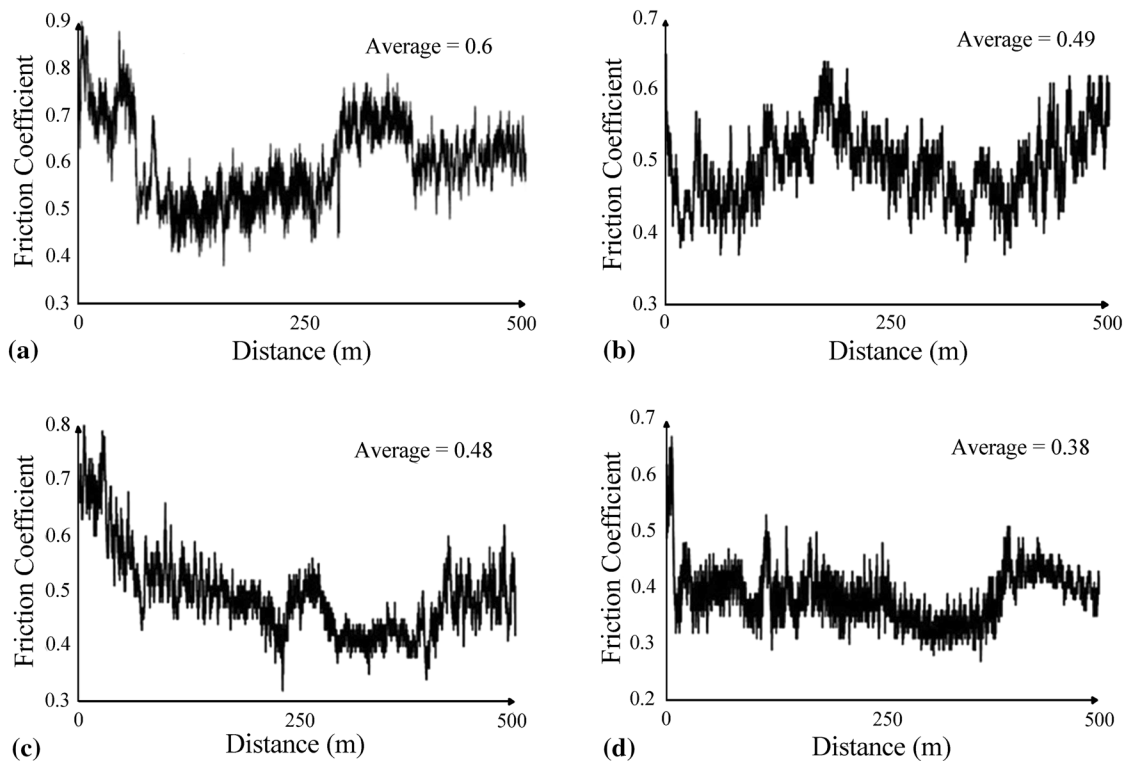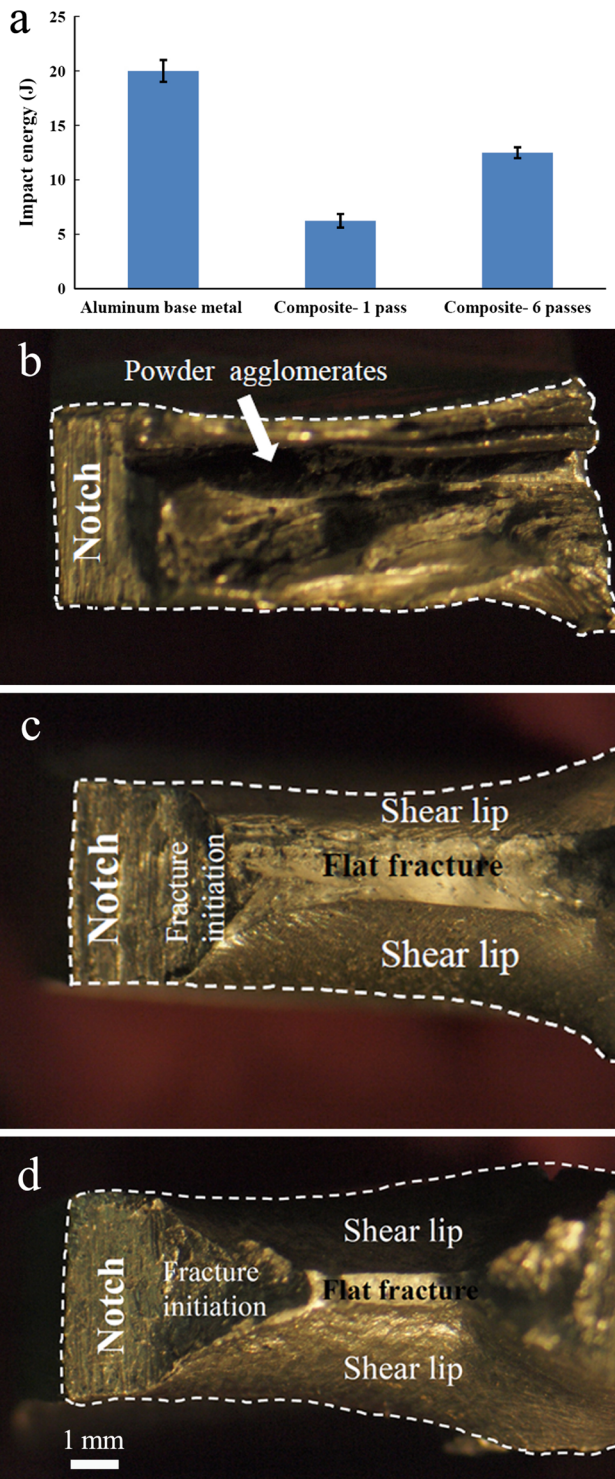
Fig. 13 Friction coefficient of (a) the base metal and the specimens processed by (b) 1 pass, (c) 3 passes and (d) 6 passes as a function of sliding distance

can improve the wear properties. According to Fig. 11(d), there were not any cracks or delamination on the worn-out surface of the specimen processed by 6 pass indicating that the wear mechanism changed from severe wear to mild wear. Besides the improvement in the reinforcing particles distribution and increase in the amount of Al-Fe intermetallic compounds with enhancement of the pass number, formation of a solid lubricated layer called as "mechanically mixed layer" (MML) affects greatly the wear behavior of the composites (Ref 38-40). This layer is produced by transfer and mixing of the materials from the pin and the disk on the pin surface. Compared to the surface of the composite, MML has higher hardness because of mechanical alloying and strain hardening. Furthermore, formation of MML may increase the thickness of the material. These phenomena can result in higher wear resistance of the composite in which this layer has been firmly formed, i.e., composites formed by 6 passes of FSP (Ref 39, 40). In order to recognize the formation of MML, the worn-out surfaces of the pins were observed at higher magnification as shown in Fig. 12 for the sample processed by 1 and 6 passes. Presence of regions with bright contrast containing high weight percent of Fe and Cr atoms (Fig. 12b and c) confirms transfer of iron and chrome from the disk to the pin surface during wear test. So, the formed MML consisted of not only aluminum, Fe_3O_4, and intermetallic compounds from the composite material but also iron and other alloying elements from the counterface steel. High weight loss in the specimens processed by 1 to 3 passes may also be attributed to lack of formation of a stable MML on the pin surface. Actually, the severe wear in theses specimens removes continuously the MML (Ref 39). Figure 12(a) shows the lack of MML on the worn-out surface of the composite processed by 1 pass. Consequently, it seems
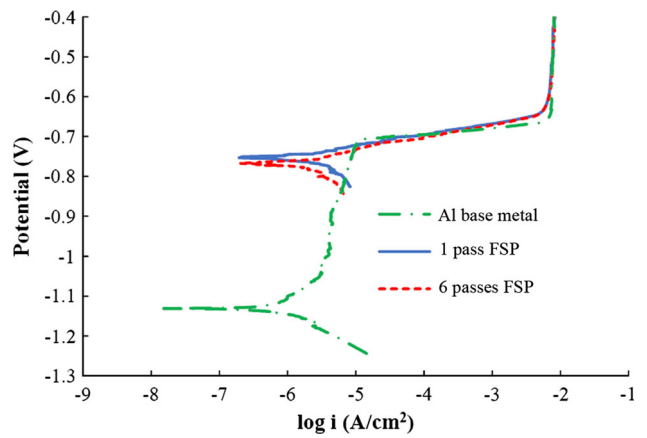
that the uniformity of the composite influences the stability of the MML. Some previous researches (Ref 40) suggested that the wear resistance of the AMCs depended on the stability of the formed MML rather than the type and amount of the reinforcing particles. When the reinforcing particles were not dispersed consistently, the volume percent of the particles varied in different regions and the regions with low volume percent of reinforcing particles could not hold the MML and therefore were severely worn.

Figure 13 shows the friction coefficient of the base metal and the composites as a function of sliding distance. In the initial distances, the friction coefficient was high due to the mismatch (different roughness) between surfaces of the pin and disk. This part is called running in stage (Ref 37). Another issue was fluctuation of the friction coefficients along the path. Formation and removing of the oxide film may be one of the reasons. When wear happens in an oxidative atmosphere; on account of high temperature generated by friction during wear, the rate of oxidation increases and an oxide layer forms on the surface. Presence of this layer decreases the friction coefficient. On the other hand, because of the imposed forces during the wear test, the oxide layer is broken, and due to higher adhesion between two virgin metals compared to a metal and an oxide film, the friction coefficient increases again (Ref 37). Separation of the reinforcing particles from the aluminum matrix and also wear debris which stay between the surfaces of the pin and disk may be another reason for fluctuation in the friction coefficient (Ref 38). Consequently, in the specimen processed by 1 pass which does not have a good bonding between the matrix and the agglomerated Fe_3O_4 particles, there are significant fluctuations in the friction coefficient. Figure 13 also reveals that compared to the aluminum base metal, the

Fig. 15 Tafel plot of the aluminum base metal and composites processed by 1 and 6 passes of FSP

3.2.4 Impact Energy. The impact energy of the samples is given in Fig. 14(a). As can be seen, the absorbed energy of the composites was lower than that of the aluminum base metal. The lower impact energy of the composites compared to the aluminum base metal may be attributed to the presence of brittle Fe_3O_4 powders as well as the in situ formed Al-Fe intermetallic particles. In comparison with the composites, the larger area of shear lips and smaller area of flat fracture in the aluminum base metal (Fig. 14d) confirm the more ductile fracture with higher absorbed energy during the impact test. However, the impact energy of the composite produced by 6 passes of FSP was significantly higher than that of the composite produced by 1 pass and reached up to ~65% of the impact energy of the annealed aluminum base metal. Figure 14(b) shows the agglomerated reinforcing particles on the fracture surface of the composite produced by 1 pass of FSP after impact test. Agglomerated particles as well as poor bonding and cracks around them inside the aluminum matrix (as discussed in section 3.1.1) may be responsible for the very low absorbed energy in these samples. Consequently, more homogenous distribution of the Fe_3O_4 particles and less defects at the stir zone of the composite produced by 6 passes of FSP led to fracture with higher absorbed energy during impact test.

3.3 Corrosion Behavior

Typical polarization curves for aluminum base metal and the composites processed by 1 and 6 passes are shown in Fig. 15. In the presence of Fe_3O_4 nanoparticles, the corrosion current of the composites changed from ~9.38×10^{-8} in the aluminum base metal to ~2.36×10^{-7} A cm^{-2} in the composite processed by 1 pass. Moreover, the corrosion potential was shifted ~0.36 V to more noble potentials in the composite processed by 1 pass compared to the aluminum base metal. More FSP passes did not influence the corrosion current significantly. However, the corrosion potential was shifted slightly to more cathodic potentials probably due to the finer grain structure. These observations showed that Fe_3O_4 reinforced composites have higher corrosion resistance in comparison with the aluminum base metal. However, observed increase in the corrosion current for composites was assigned to possible electrochemical coupling between Fe_3O_4 particles/Al-Fe intermetallic compounds and the aluminum matrix. On the other hand, with enhancement of the over-potential, the initial formed

Fig. 14 (a) Absorbed impact energy. Stereographs from the fracture surface of (b) composite processed by 1 pass, (c) composite processed by 6 pass and (d) aluminum base metal

composites show lower values of the average friction coefficient. Moreover, with increasing the pass number leading to higher hardness and lower weight loss, the friction coefficient decreases. Friction coefficient of the composite processed by 6 passes is ~37% lower than that of the base metal.

passive layer on the surface of aluminum base metal stared to be broken down at about -0.71 V versus SCE (trans-passive potential). Subsequently, pitting corrosion got induced. Pitting corrosion led to higher current density of small pits (or pit groups) compared to the passive surface. Interestingly, the observed pitting corrosion in aluminum base metal was not detected in the presence of Fe_3O_4 nanoparticles. This may be due to the presence of Al_3Fe and Al_5Fe_2 intermetallics which act as cathodes with respect to metal matrix (Ref 41, 42) and enhance pitting corrosion resistance. The improved pitting behavior is more important in presence of chloride ions, when the aluminum surface gets very sensitive to pitting corrosion (Ref 43). Therefore, it can be concluded that Fe_3O_4 nanoparticles had a dual effect on the corrosion resistance of the aluminum base metal. Formation of composite was shifted the corrosion potential to more noble potentials and improved pitting corrosion resistance. However, corrosion current for composites increased because of the electrochemical coupling between Fe_3O_4 particles/intermetallic compounds and aluminum matrix.

4. Conclusion

Al matrix/IMC in situ nanocomposite was produced using friction stir processing. The results can be summarized as follows:

1. In situ aluminum nanocomposite with Fe_3O_4 and Al-Fe intermetallics reinforcements was successfully produced using friction stir processing.
2. Because of high temperature and severe plastic deformation experienced by the stir zone, conditions for the reduction of Fe_3O_4 particles as well as the interdiffusion of Al and Fe atoms through the interface of the particle/matrix were provided and therefore, Al_3Fe and Al_5Fe_2 were formed. Subsequently, this reaction layer was broken up and dispersed in the aluminum matrix by the stirring action of the rotating tool. Nanometer particles (broken intermetallics and/or Fe_3O_4 powders) with the size <100 nm were observed in the composite processed by six passes.
3. Increase in the FSP pass number from one to six passes led to the finer grain structure, more homogenous distribution of the reinforcing particles and less defects at the stir zone. Consequently, the hardness and UTS of the composites were increased 64 and 27%, respectively, compared to the base metal.
4. The very low elongation of the composites processed by one pass was related to the dominance of brittle features on the fracture surface. However, in the composites processed with pass number higher than three passes, a mixture of ductile and brittle features was observed on the fracture surfaces.
5. Formation and removal of the MML affecting the wear resistance of the composite depended on the uniformity of the reinforcing particles distribution. Thus, a stable MML was detected only on the worn-out surface of the specimen processed by 6 passes.
6. The wear resistance of all nanocomposites was higher than that of the base metal. Increase in the FSP pass number improved the wear resistance due to the forma-

tion of the MML and more uniform distribution of the reinforcing particles which changed the severe wear to mild wear.
7. Impact energy of the composites was lower than that of the aluminum base metal due to the presence of brittle Fe_3O_4 and Al-Fe intermetallic particles. However, the impact energy of the composite produced by 6 passes of FSP was higher than that of the composite produced by 1 pass and reached up to $\sim 65\%$ of the impact energy of the annealed aluminum base metal.
8. In composites, corrosion potential changed to more noble potentials and pitting corrosion resistance improved. However, corrosion current for composites increased because of the electrochemical coupling between Fe_3O_4 particles/intermetallic compounds and aluminum matrix.

References

1. W.F. Smith, *Structure and Properties of Engineering Alloys*, 2nd ed., McGraw-Hill, New York, 1994, p 176–184
2. G. Hussain, R. Hashemi, H. Hashemi, and K.A. Al-Ghamdi, An Experimental Study on Multi-pass Friction Stir Processing of Al/TiN Composite: Some Microstructural, Mechanical, and Wear Characteristics, *Int. J. Adv. Manuf. Technol.*, 2016, **84**, p 533–546
3. Y. Zhao, X. Huang, Q. Li, J. Huang, and K. Yan, Effect of Friction Stir Processing with B_4C Particles on the Microstructure and Mechanical Properties of 6061 Aluminum Alloy, *Int. J. Adv. Manuf. Technol.*, 2016, **78**, p 1437–1443
4. O. Culha, C. Tekmen, M. Toparli, and Y. Tsunekawa, Mechanical Properties of In Situ Al_2O_3 Formed Al-Si Composite Coating Via Atmospheric Plasma Spraying, *Mater. Des.*, 2010, **31**, p 533–544
5. O. Verezub, Z. Kálazi, G. Buza, N.V. Verezub, and G. Kaptay, In-Situ Synthesis of a Carbide Reinforced Steel Matrix Surface Nanocomposite by Laser Melt Injection Technology and Subsequent Heat Treatment, *Surf. Coat. Technol.*, 2009, **203**, p 3049–3057
6. S.M. Ma, P. Zhang, G. Ji, Z. Chen, G.A. Sun, S.Y. Zhong, V. Ji, and H.W. Wang, Microstructure and Mechanical Properties of Friction Stir Processed Al-Mg-Si Alloys Dispersion-Strengthened by Nanosized TiB_2 Particles, *J. Alloys Compd.*, 2014, **616**, p 128–136
7. R.S. Mishra and Z.Y. Ma, Friction Stir Welding and Processing, *Mater. Sci. Eng. R*, 2005, **50**, p 1–78
8. M.H. Razmpoosh, A. Zarei-Hanzaki, S. Heshmati-Manesh, S.M. Fatemi-Varzaneh, and A. Marandi, The Grain Structure and Phase Transformations of TWIP Steel During Friction Stir Processing, *J. Mater. Eng. Perform.*, 2015, **24**(7), p 2826–2835
9. J. Jafari, M.K. Besharati Givi, and M. Barmouz, Mechanical and Microstructural Characterization of Cu/CNT Nanocomposite Layers Fabricated Via Friction Stir Processing, *Int. J. Adv. Manuf. Technol.*, 2015, **78**, p 199–209
10. M. Barmouz, M.K. Besharati Givi, and J. Jafari, Evaluation of Tensile Deformation Properties of Friction Stir Processed Pure Copper: Effect of Processing Parameters and Pass Number, *J. Mater. Eng. Perform.*, 2014, **23**(1), p 101–107
11. R. Mishra, Z. Ma, and I. Charit, Friction Stir Processing: A Novel Technique for Fabrication of Surface Composite, *Mater. Sci. Eng. A*, 2003, **341**, p 307–310
12. B. Hekner, J. Myalski, N. Valle, A. Botor-Probierz, M. Sopicka-Lizer, and J. Wieczorek, Friction and Wear Behavior of Al-SiC(n) Hybrid Composites with Carbon Addition, *Compos. Part B Eng.*, 2017, **108**, p 291–300. doi:10.1016/j.compositesb.2016.09.103
13. R. Palanivel, I. Dinaharan, R.F. Laubscher, and J.P. Davim, Influence of Boron Nitride Nanoparticles on Microstructure and Wear Behavior of AA6082/TiB_2 Hybrid Aluminum Composites Synthesized by Friction Stir Processing, *Mater. Des.*, 2016, **106**, p 195–204
14. D. Yadav and R. Bauri, Friction Stir Processing of Al-TiB2 In Situ Composite: Effect on Particle Distribution, Microstructure and Properties, *J. Mater. Eng. Perform.*, 2015, **24**(3), p 1116–1124

15. S.R. Anvari, F. Karimzadeh, and M.H. Enayati, A Novel Route for Development of Al-Cr-O Surface Nano-composite by Friction Stir Processing, *J. Alloys Compd.*, 2013, **562**, p 48–55

16. J.M. Lee, S.B. Kang, T. Sato, H. Tezuka, and A. Kamiob, Evolution of Iron Aluminide in Al/Fe In Situ Composites Fabricated by Plasma Synthesis Method, *Mater. Sci. Eng. A*, 2003, **362**, p 257–263

17. J. Gu, S. Gu, L. Xue, S. Wu, and Y. Yan, Microstructure and Mechanical Properties of In-situ $Al_{13}Fe_4$/Al Composites Prepared by Mechanical Alloying and Spark Plasma Sintering, *Mater. Sci. Eng. A*, 2012, **558**, p 684–691

18. I.S. Lee, P.W. Kao, and N.J. Ho, Microstructure and Mechanical Properties of Al-Fe In Situ Nanocomposite Produced by Friction Stir Processing, *Intermetallics*, 2008, **16**, p 1104–1108

19. M. SarkariKhorrami, S. Samadi, Z. Janghorban, and M. Movahedi, In-situ Aluminum Matrix Composite Produced by Friction Stir Processing Using FE Particles, *Mater. Sci. Eng. A*, 2015, **641**, p 380–390

20. http://www.us-nano.com/inc/sdetail/16809. Accessed 26 Jan 2017

21. D.R. Gaskell, *Introduction of thermodynamics of materials*, 4th ed., Taylor & Francis e-Library pub, Abingdon, 2009, p 412–430

22. M. Movahedi, A.H. Kokabi, S.M. Seyed Reihani, H. Najafi, S.A. Farzadfar, W.J. Cheng, and C.J. Wang, Growth Kinetics of Al-Fe Intermetallic Compounds During Annealing Treatment of Friction Stir Lap Welds, *Mater. Charact.*, 2014, **90**, p 121–126

23. W. Xingqing, J.V. Wood, S. Yongjiang, and L. Haibo, Formation of Intermetallic Compound in Iron-Aluminum Alloys, *J. Shanghai Univ.*, 2014, **2**, p 305–310

24. N. Hansen and B. Bay, Initial Stages of Recrystallization in Aluminum Containing Both Large and Small Particles, *Acta Metall.*, 1981, **29**, p 65–77

25. R.D. Doherty, D.A. Hughes, F.J. Humphreys, J.J. Jonas, D. Juul Jensen, M.E. Kassner, W.E. King, T.R. McNelley, H.J. McQueen, and A.D. Rollett, Current Issues in Recrystallization: A Review, *Mater. Sci. Eng. A*, 1997, **238**, p 219–274

26. C.J. Hsu, C.Y. Chang, P.W. Kao, N.J. Ho, and C.P. Chang, Al-Al_3Ti Nanocomposites Produced In Situ by Friction Stir Processing, *Acta Mater.*, 2006, **54**, p 5241–5249

27. M. Sarkari Khorrami, M. Kazeminezhad, and A.H. Kokabi, The Effect of SiC Nanoparticles on the Friction Stir Processing of Severely Deformed Aluminum, *Mater. Sci. Eng. A*, 2014, **602**, p 110–118

28. E.O. Hall, The Deformation and Ageing of Mild Steel: III, Discussion of Results, *Proc. Phys. Soc. B*, 1951, **64**, p 747–753

29. N.J. Petch, The Cleavage Strength of Polycrystals, *J. Iron Steel Inst.*, 1953, **147**, p 25–28

30. D. Tabor, The Hardness and Strength of Metals, *J. Inst. Metals*, 1951, **79**, p 1–18

31. T. Shanmugasundaram, M. Heilmaier, B.S. Murty, and V. Subramanya Sarma, On the Hall–Petch Relationship in a Nanostructured Al-Cu Alloy, *Mater. Sci. Eng. A*, 2010, **527**, p 7821–7825

32. M. Khajouei-Nezhad, M.H. Paydar, R. Ebrahimi, P. Jenei, P. Nagy, and J. Gubicza, Microstructure and Mechanical Properties of Ultrafine-Grained Aluminum Consolidated by High-Pressure Torsion, *Mater. Sci. Eng. A*, 2017, **682**, p 501–508

33. C.R. Bradbury, J.-K. Gomon, L. Kollo, H. Kwon, and M. Leparoux, Hardness of Multi Wall Carbon Nanotubes Reinforced Aluminium Matrix Composites, *J. Alloys Compd.*, 2014, **585**, p 362–367

34. Y.S. Sato, M. Urata, H. Kokawa, and K. Ikeda, Hall–Petch Relationship in Friction Stir Welds of Equal Channel Angular-Pressed Aluminium Alloys, *Mater. Sci. Eng. A*, 2003, **354**, p 298–305

35. N.P. Suh, The Delamination Theory of Wear, *Wear*, 1973, **25**, p 111–124

36. R.L. Deuis, C. Subramanian, and J.M. Yellupb, Dry Sliding Wear of Aluminium Composites-A Review, *Compos. Sci. Technol.*, 1997, **57**, p 415–435

37. B. Bhushan, *Modern Tribology Handbook*, CRC Press LLC, Florida, 2001, p 1–1728

38. E.R.I. Mahmoud, M. Takahashi, T. Shibayanagi, and K. Ikeuchi, Wear Characteristics of Surface-Hybrid-MMCs Layer Fabricated on Aluminum Plate by Friction Stir Processing, *Wear*, 2010, **268**, p 1111–1121

39. B. Venkataraman and G. Sundararajan, Correlation Between the Characteristics of the Mechanically Mixed Layer and Wear Behavior of Aluminum, Al-7075 Alloy and Al-MMCs, *Wear*, 2000, **245**, p 22–38

40. M.R. Rosenberger, E. Forlerer, and C.E. Schvezov, Wear of Different Aluminum Matrix Composites Under Conditions that Generate a Mechanically Mixed Layer, *Wear*, 2005, **259**, p p590–p601

41. N. Birbilis and R.G. Buchheit, Electrochemical Characteristics of Intermetallic Phases in Aluminum Alloys, *J. Electrochem. Soc.*, 2005, **152**(4), p B140–B151

42. M.K. Cavanaugh, J.-C. Li, N. Birbilis, and R.G. Buchheit, Electrochemical Characterization of Intermetallic Phases Common to Aluminum Alloys as a Function of Solution Temperature, *J. Electrochem. Soc.*, 2014, **161**(12), p C535–C543

43. H.C. Ananda Murthy and S.K. Singh, Influence of TiC Particulate Reinforcement on the Corrosion Behaviour of Al 6061 Metal Matrix Composites, *Adv. Mater. Lett.*, 2015, **6**(7), p 633–640